J. Fluid Mech. (2010), *vol.* 657, *pp.* 478–501.
doi:10.1017/S0022112010001515

Moist multi-scale models for the hurricane embryo

ANDREW J. MAJDA[1]†, YULONG XING[2,3] AND MAJID MOHAMMADIAN[4]

[1]Department of Mathematics and Climate, Atmosphere and Ocean Science, Courant Institute of Mathematical Sciences, New York University, New York, NY 10012, USA

[2]Computer Science and Mathematics Division, Oak Ridge National Laboratory, Oak Ridge, TN 37831, USA

[3]Department of Mathematics, University of Tennessee, Knoxville, TN 37996, USA

[4]Department of Civil Engineering, University of Ottawa, Ontario, Canada K1N 6N5

(Received 26 March 2009; revised 22 March 2010; accepted 23 March 2010; first published online 30 June 2010)

Determining the finite-amplitude preconditioned states in the hurricane embryo, which lead to tropical cyclogenesis, is a central issue in contemporary meteorology. In the embryo there is competition between different preconditioning mechanisms involving hydrodynamics and moist thermodynamics, which can lead to cyclogenesis. Here systematic asymptotic methods from applied mathematics are utilized to develop new simplified moist multi-scale models starting from the moist anelastic equations. Three interesting multi-scale models emerge in the analysis. The balanced mesoscale vortex (BMV) dynamics and the microscale balanced hot tower (BHT) dynamics involve simplified balanced equations without gravity waves for vertical vorticity amplification due to moist heat sources and incorporate nonlinear advective fluxes across scales. The BMV model is the central one for tropical cyclogenesis in the embryo. The moist mesoscale wave (MMW) dynamics involves simplified equations for mesoscale moisture fluctuations, as well as linear hydrostatic waves driven by heat sources from moisture and eddy flux divergences. A simplified cloud physics model for deep convection is introduced here and used to study moist axisymmetric plumes in the BHT model. A simple application in periodic geometry involving the effects of mesoscale vertical shear and moist microscale hot towers on vortex amplification is developed here to illustrate features of the coupled multi-scale models. These results illustrate the use of these models in isolating key mechanisms in the embryo in a simplified content.

1. Introduction

Hurricanes or tropical cyclones do not form spontaneously and involve a hurricane embryo. The embryo is a localized region where simultaneously a deep cloud cluster forms and low-level cyclonic vorticity amplifies. The embryo requires finite-amplitude preconditioning involving typically a mesoscale low pressure trough for the ambient background flow, as well as the thermodynamic preconditioning of a moist lower troposphere with large convectively available potential energy favourable to deep convection, and a sufficiently large sea surface temperature (Emanuel 1989). The

† Email address for correspondence: majda@cims.nyu.edu

ambient background preconditioning flow often involves a weak cyclonic vortex in a weak background shear (Molinari, Vollaro & Corbosiero 2004; Frank & Roundy 2006; Molinari, Lombardo & Vollaro 2007) and the transition to a mature cyclone involves complex multi-scale interaction (Ritchie & Holland 1997).

One group has emphasized a turbulent vortical hot tower route for cyclogenesis in the embryo (Hendricks, Montgomery & Davis 2004; Montgomery *et al.* 2006) and the role of critical layers in the background flow (Dunkerton, Montgomery & Wang 2008). Others have given a dominant role to moist thermodynamics (Nolan 2007, and references therein) in the preconditioned environment. Recent work (Hendricks *et al.* 2004; Montgomery *et al.* 2006) involving numerical simulation of comprehensive mesoscale models suggests that deep convection enhances low-level cyclonic rotation through the merger of rotating updrafts. The present paper involves a new family of simplified moist multi-scale models which are useful in sorting out the fluid dynamical and moist thermodynamic contributions in tropical cyclogenesis as well as isolating the prominent dynamical mechanisms in the process in a simplified context. For example, § 4 illustrates that the present models have simplified moist axisymmetric hot towers which respond in a qualitatively correct fashion to increasing low-level background moisture. The simulations in § 5 illustrate the development of intense low-level cyclonic vorticity fluctuations through moist balanced hot towers (BHTs) with simplified cloud physics.

The spatial and temporal scales for the development of deep convective moist hot towers, called the microscales here, have the units

$$L_m = 10\,\mathrm{km}, \qquad T_m = 15\,\mathrm{min}. \tag{1.1}$$

The spatiotemporal scales for the development of intensifying mesoscale vortices in the hurricane embryo are the mesoscales with units

$$L_M = 100\,\mathrm{km} = \epsilon^{-1} L_m, \qquad T_M = 2.5\,\mathrm{h} = \epsilon^{-1} T_m \tag{1.2}$$

for $\epsilon \approx 0.1$. The parameter ϵ also simultaneously represents the low Froude number $\epsilon = Fr = v/(N L_m)$ based on the 10 km length scale in a distinguished asymptotic limit with the typical velocity of 10 m s^{-1} and the standard atmosphere value for the Brunt–Väisälä frequency $N = 10^{-2}\,s^{-1}$. See the discussion below (2.3) in § 2. On the larger time scale T_M, the effects of rotation become significant. The main goal of the present paper is to develop simplified moist multi-scale models involving the scales in (1.1) and (1.2) which involve the upscale and downscale vortical and moist thermodynamic processes governing the hurricane embryo. These simplified models are developed here by utilizing systematic multi-scale asymptotic methods from applied mathematics (Klein 2000; Majda 2003; Majda & Klein 2003; Klein & Majda 2006; Majda 2007*a*,*b*; Biello & Majda 2009; Majda & Xing 2009). Such simplified multi-scale models have already proved to be useful in understanding the multi-scale features of tropical inter-seasonal oscillations (Majda & Biello 2004; Biello & Majda 2005, 2006; Biello, Majda & Moncrieff 2007; Majda & Stechmann 2009), the self-similarity of convectively coupled waves in the tropics (Majda 2007*b*), the propagation of squall lines in strong vertical shear (Majda & Xing 2009) and for supplying a systematic framework (Majda 2007*b*) for improving superparameterization algorithms (Grabowski 2001, 2004; Xing, Majda & Grabowski 2009). The crucial additional assumption in the asymptotic derivation presented below is sufficiently low Froude numbers which allow horizontal velocities of order 10 m s^{-1}; this simplifying assumption is natural for the hurricane embryo with weak preconditioned shear and vortices and allows for the development of intense mesoscale vortices in the transition

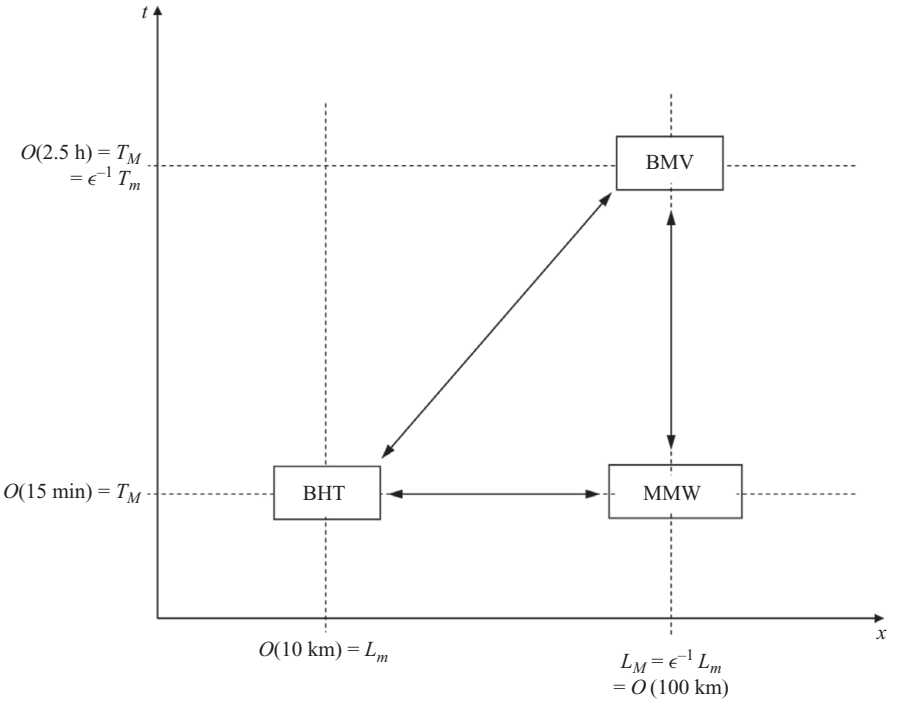

FIGURE 1. The multiple spatiotemporal scales spanned by the interacting multi-scale models in the embryo.

to cyclogenesis. Obviously, the complete final transition to a mature hurricane involves even stronger winds which violate this assumption. The simplified multi-scale models are developed in the context of the moist anelastic equations with warm rain bulk cloud microphysics; § 2 contains a discussion of the non-dimensionalization of these equations as well as an introduction to the multi-scale asymptotics needed in this paper. The moist multi-scale equations for the hurricane embryo are derived and discussed in § 3. A simplified cloud physics scheme for deep convection is introduced in § 4 and utilized there to study moist axisymmetric plumes in the BHT models. Section 5 contains a simple application in periodic geometry involving the effects of mesoscale vertical shear and moist microscale hot towers on vortex intensification. Concluding discussion follows in § 6. Next, we provide a brief summary of the simplified multi-scale asymptotic models for the hurricane embryo derived in § 3; this summary should be useful for those readers who are not interested in all the technical details.

1.1. *Simplified multi-scale model for the hurricane embryo*

The multi-scale model consists of three simplified dynamical models which interact on the time scales in (1.1) and (1.2), and are depicted schematically in figure 1. The BHT model which operates on the microscale in (1.1) (see § 3.1) and the balanced mesoscale vortex (BMV) model which operates on the mesoscales in (1.2) (see § 3.3) involve active moisture dynamics coupled with vertical vorticity dynamics but the gravity waves on these scales, respectively, are systematically removed. Besides moisture processes, the dynamical core for both the BHT and BMV models involves the simplified canonical

balanced model

$$\left.\begin{aligned} \frac{\mathrm{D}\boldsymbol{u}_h}{\mathrm{D}t} + f\boldsymbol{u}_h^{\perp} &= -\nabla_h p + \boldsymbol{F}_{\boldsymbol{u}}, \\ N^2(z)w &= S_\theta, \\ \nabla_h \cdot \boldsymbol{u}_h + w_z &= 0, \end{aligned}\right\} \tag{1.3}$$

where $N(z)$ is the buoyancy frequency and S_θ and $\boldsymbol{F}_{\boldsymbol{u}}$ are mass (heat) and momentum sources, respectively. In (1.3), $(\boldsymbol{u}_h, w) = (u, v, w)$ is the total velocity where $\mathrm{D}/\mathrm{D}t = \partial/\partial t + \boldsymbol{u}_h \cdot \nabla_h + w\partial/\partial z$, $\boldsymbol{u}_h^{\perp} = (-v, u)^T$, f is a constant non-dimensional vertical rotation component and $\nabla_h \cdot$ and ∇_h are the horizontal divergence and gradient. Vorticity amplification in the canonical balanced model in (1.3) with prescribed heat sources as well as elementary models for the hurricane embryo are discussed systematically in Majda, Mohammadian & Xing (2008). In both the BHT and BMV models, the heat sources are determined by suitable fluctuations and space–time averages, respectively, from the moist processes.

The embryo consists of both the large-scale variables and the small-scale variables in BHT. The BMV model provides both the large-scale ambient flow environment for the embryo as well as the model to observe the transition to cyclogenesis; both the effects of rotation, $f \neq 0$, and three-dimensional self-advection are non-zero in the BMV model while the momentum forcing $\boldsymbol{F}_{\boldsymbol{u}}$ contains turbulent eddy flux divergences from both the BHT model and the moist mesoscale wave (MMW) model. The BMV model contains the competition between both the effect of moisture processes and the upscale mechanical turbulent transport processes as well as nonlinear advection in a simplified balanced model for the transition to cyclogenesis.

The BHT model for the fluctuations on the microscales in (1.1) is a version of (1.3) with $f \equiv 0$ but crucially the nonlinear advection of horizontal momentum contains horizontal advection by the BMV and MMW models as well as self-advection; similarly, the fluctuating source terms, S_θ, in (1.3) for the BHT model involve heating from moist processes that is effected by the large-scale moist background profile in MMW and BMV. See §4 on moist axisymmetric plumes in the BHT model for a simple illustration. Both the BHT and BMV models exploit simplified dynamics which is valid on the scales in (1.1) and (1.2) (Sobel, Nilsson & Polvani 2001; Majda *et al.* 2008).

The MMW model operates on the mesoscale length scale in (1.2) but the more rapid time scale in (1.1) (see figure 1 and §3.2); the MMW model involves simplified mesoscale fluctuations of moisture as well as linear hydrostatic gravity wave motion driven by heat sources from moisture and fluctuations from eddy flux divergences of momentum from BHT. The MMW model allows for a simplified assessment of mesoscale gravity waves driven by moisture processes in the embryo.

2. Preliminary background

2.1. *The moist anelastic equations*

Here the moist non-hydrostatic anelastic equations with bulk cloud microphysics (Lipps & Hemler 1982; Grabowski & Smolarkiewicz 1996) are utilized as the basic equations for the microscale dynamics. With suitable non-dimensional units explained below (Klein & Majda 2006), which have the space-time scales

$$L_m = 10\,\mathrm{km} \qquad \text{and} \qquad T_m = 15\,\mathrm{min}, \tag{2.1}$$

with

$$[\boldsymbol{u}_h] = [w] = 10\,\mathrm{m\ s^{-1}},$$

these equations are given by the dynamical core

$$\left.\begin{aligned} \frac{\mathrm{D}\boldsymbol{u}_h}{\mathrm{D}t} + \epsilon f \boldsymbol{u}^{\perp} &= -\nabla_h p, \\ \frac{\mathrm{D}w}{\mathrm{D}t} &= -p_z + \epsilon^{-1}\theta + (\bar{\epsilon} q_v - q_r - q_c), \\ \frac{\mathrm{D}\theta}{\mathrm{D}t} + N^2(z)\epsilon^{-1} w &= \epsilon^{-1} L \frac{\theta_0}{p_0}(C_d - E_r), \\ \mathrm{div}_h \boldsymbol{u}_h + \rho^{-1}(\rho w)_z &= 0 \end{aligned}\right\} \tag{2.2}$$

with

$$\frac{\mathrm{D}}{\mathrm{D}t} = \frac{\partial}{\partial t} + \boldsymbol{u}_h \cdot \nabla_h + w\frac{\partial}{\partial z},$$

and the cloud dynamic equations

$$\left.\begin{aligned} \frac{\mathrm{D}q_v}{\mathrm{D}t} &= -C_d + E_r, \\ \frac{\mathrm{D}q_c}{\mathrm{D}t} &= C_d - A_r, \\ \frac{\mathrm{D}q_r}{\mathrm{D}t} - \frac{1}{\rho}\frac{\partial}{\partial z}(\rho V_T q_r) &= A_r - E_r. \end{aligned}\right\} \tag{2.3}$$

In (2.2), $\rho(z)$, $N^2(z)$, $\theta_0(z)$ and $p_0(z)$ are the non-dimensional versions of the dry statically stable vertical profile (Majda & Klein 2003; Klein & Majda 2006). Here $\bar{\epsilon} + 1$ is the ratio of gas constants of water vapour and dry air. The Froude number $\epsilon = v/(NL_m)$ is $O(\epsilon)$ with the typical velocity of $10\,\mathrm{m\ s^{-1}}$, the length scale L_m of 10 km and the standard atmosphere value $N = 10^{-2}\,\mathrm{s^{-1}}$. The potential temperature in (2.2) is scaled as a small deviation from hydrostatic balance; that is, the units of θ are 3 K, which compares with a dry lapse rate of 30 K over 10 km; thus $\epsilon \approx 0.1$ in (2.2) (see Klein & Majda 2006; Majda 2007*a*; Majda *et al.* 2008, for detailed information). On the 15 min time scale in (2.1), the effect of rotation is weak. This is reflected in the horizontal momentum equation in (2.2) where the term ϵf is the vertical component of the Coriolis effect of rotation in these time units with $f = \sin\phi$ and ϕ a given latitude (Klein 2000). The quantities q_v, q_c and q_r are the mixing ratios for cloud vapour, water and rain, respectively, rescaled by the factor ϵ^{-2}. This rescaling developed in Klein & Majda (2006) renders the potential temperature equation in (2.2) dimensionless with order 1 latent heat prefactor L and simultaneously guarantees that the condensation of cloud vapour, C_d, evaporation of rain, E_r, and the conversion of cloud water to rain by both autoconversion and collection, A_r, as well as the fall velocity, V_T, are order 1 processes on the time scales in (2.1). While the detailed forms of C_d, E_r and A_r (Emanuel 1994; Grabowski & Smolarkiewicz 1996) are not needed for the discussion here, the tacit standard assumption utilized in achieving a single time scale governing the moisture source terms in (2.2) and (2.3) is that the very fast processes associated with supersaturated water vapour are equilibrated by constraining the cloud vapour to always lie below or equal to saturation (Lipps & Hemler 1982; Grabowski & Smolarkiewicz 1996; Klein & Majda 2006). For simplicity in exposition, all other

Parameter	Units	Description
L	10 km	Length scale
t	15 min	Time scale
u, w	10 km/15 min $\approx$ 10 m s^{-1}	Horizontal and vertical velocity scale
θ	3 K	Potential temperature scale

TABLE 1. The basic units for non-dimensionalization.

source terms and dissipation in (2.2) and (2.3) have been set to zero; they are readily added in the analysis below.

The basic non-dimensional units are listed in table 1. The heat release from moisture on these microscales can be very strong, of order 30 K/15 min. Such large values are actually consistent with the hot towers on 10 km scales present in the hurricane embryo (Hendricks *et al.* 2004; Montgomery *et al.* 2006). The order 10 m s^{-1} horizontal velocities allow for significant acceleration of the winds as well as moderate shear which are both features of the embryo.

2.2. *Multiple scale asymptotics*

Here the focus is on systematic multi-space/multi-time scale asymptotic solutions of (2.2) and (2.3) on the microscales in (2.1) and mesoscales, L_M and T_M, with

$$L_M = \epsilon^{-1} L_m = 100\,\mathrm{km}, \qquad T_M = \epsilon^{-1} T_m = 2.5\,\mathrm{h}. \tag{2.4}$$

With (2.1) and (2.4) as the essential spatiotemporal scales, general asymptotic solutions of (2.2), (2.3) are developed with the form

$$\left.\begin{aligned} \boldsymbol{u}_h &= \bar{\boldsymbol{u}}_h(\epsilon\boldsymbol{x}, z, \epsilon t, t) + \boldsymbol{u}'_h(\epsilon\boldsymbol{x}, \boldsymbol{x}, z, \epsilon t, t) + \epsilon(\bar{\boldsymbol{u}}_{h,1} + \boldsymbol{u}'_{h,1}) + O(\epsilon^2),\\ w &= w' + \epsilon(\bar{w}_1 + w'_1) + O(\epsilon^2),\\ \theta &= \tilde{\bar{\theta}} + \epsilon(\langle\bar{\theta}_1\rangle + \theta'_1) + O(\epsilon^2),\\ p &= \epsilon^{-1}\tilde{\bar{p}}_{-1} + (\langle\bar{p}\rangle + p') + O(\epsilon),\\ \boldsymbol{q} &= \bar{\boldsymbol{q}} + \boldsymbol{q}' + \epsilon(\bar{\boldsymbol{q}}_1 + \boldsymbol{q}'_1) + O(\epsilon^2), \end{aligned}\right\} \tag{2.5}$$

where $\boldsymbol{q} = (q_v, q_c, q_r)$. Only the central non-zero terms developed below are listed in (2.5) and the notation is developed and explained next. In (2.5) the larger scale longer space–time variables,

$$\boldsymbol{X} = \epsilon\boldsymbol{x}, \qquad T = \epsilon t, \tag{2.6}$$

account for mesoscale modulations. In accordance with conventional multiple-scale asymptotic analysis (Klein 2000; Majda 2003, 2007*a*,*b*; Klein & Majda 2006), given a general function $f(\epsilon\boldsymbol{x}, \boldsymbol{x}, \epsilon t, t)$, the spatial and time averages of f over the microscales are given, respectively, by

$$\left.\begin{aligned} \bar{f}(\boldsymbol{X}, T, t) &= \lim_{L\to\infty} \frac{1}{(2L)^2}\int_{-L}^{L}\int_{-L}^{L} f(\boldsymbol{X}, \boldsymbol{x}, T, t)\,\mathrm{d}x\,\mathrm{d}y,\\ \langle f\rangle(\boldsymbol{X}, \boldsymbol{x}, T) &= \lim_{\tilde{T}\to\infty} \frac{1}{2\tilde{T}}\int_{-\tilde{T}}^{\tilde{T}} f(\boldsymbol{X}, \boldsymbol{x}, T, t)\,\mathrm{d}t. \end{aligned}\right\} \tag{2.7}$$

With the first equation in (2.7), a function f admits the decomposition $f = \bar{f} + f'$ with $\overline{f'} = 0$ which gives a conventional separation of the terms in (2.5) into their spatial means and fluctuations. Note that the spatiotemporal average involves variations only

on the larger and longer mesoscales in (2.4), i.e.

$$\langle \bar{f} \rangle(\boldsymbol{X}, z, T). \tag{2.8}$$

For a function $f(\boldsymbol{X}, T, t)$ involving the mesoscale in space and the two time scales with time average $\langle f \rangle(\boldsymbol{X}, T)$, the fluctuations over the faster time scale are given by

$$\tilde{f}(\boldsymbol{X}, T, t) = f - \langle f \rangle. \tag{2.9}$$

From the above discussion, a general function $f(\boldsymbol{X}, \boldsymbol{x}, T, t)$ has the decomposition

$$f(\boldsymbol{X}, \boldsymbol{x}, T, t) = \langle \bar{f} \rangle(\boldsymbol{X}, T) + \tilde{\bar{f}}(\boldsymbol{X}, T, t) + f'(\boldsymbol{X}, \boldsymbol{x}, T, t). \tag{2.10}$$

Note that the z-dependence has been suppressed for simplicity in the present discussion which defines all of the terms in (2.5). In the next section, systematic asymptotic equations are developed for both the fluctuations and the mesoscale averages, $\langle \bar{\boldsymbol{u}}_h \rangle(\boldsymbol{X}, z, T)$, etc. from (2.2) and (2.3) which are the quantities of interest. In the multi-scale procedure utilized in the next section the space–time gradient of $f(\epsilon \boldsymbol{x}, \boldsymbol{x}, \epsilon t, t)$ is calculated according to the chain rule as

$$\epsilon \nabla_{\boldsymbol{X}} f + \nabla' f, \qquad \epsilon \frac{\partial f}{\partial T} + \frac{\partial f}{\partial t}, \tag{2.11}$$

where the notation $\nabla' f = (\partial f/\partial x, \partial f/\partial y)$ denotes the horizontal gradient of the fluctuations.

One of the central principles of multi-scale asymptotics is to guarantee that secular terms are suppressed in order to generate a valid asymptotic representation; simultaneously, the systematic use of these procedures guarantees that a sequence of model equations emerges from the analyses (see e.g. Klein 2000; Majda 2003; Majda & Klein 2003; Majda 2007*a*, *b*; Majda & Xing 2009). A necessary condition for the validity of the asymptotic expansion in (2.5) is that the lower-order terms grow slower than linear, sublinear, in the small-scale and fast variables $(\boldsymbol{x}, t)$. In the next section, we utilize the following elementary averaging principle to suppress such secularities: if $f(\boldsymbol{X}, \boldsymbol{x}, T, t)$ has sublinear growth then

$$\left\langle \frac{\partial f}{\partial t} \right\rangle = 0, \qquad \overline{\nabla_{\boldsymbol{x}} f} = 0. \tag{2.12}$$

The simplest illustration of these concepts is provided by the multi-scale expansion of the anelastic constraint in (2.2) given by mass conservation,

$$\mathrm{div}_{\boldsymbol{x}} \boldsymbol{u}_h + \epsilon \, \mathrm{div}_{\boldsymbol{X}} \boldsymbol{u}_h + \frac{1}{\rho}(\rho w)_z = 0. \tag{2.13}$$

By using the second solvability condition in (2.12) and taking the spatial average, we obtain

$$\epsilon \, \mathrm{div}_{\boldsymbol{X}} \bar{\boldsymbol{u}}_h + \frac{1}{\rho}(\rho \bar{w})_z = 0. \tag{2.14}$$

The only way to self-consistently solve this equation in a non-trivial fashion is to have the weaker vertical velocity,

$$\bar{w} = \epsilon \, \bar{w}_1, \tag{2.15}$$

on the mesoscales. This both justifies the ansatz for the vertical velocity in (2.5) and demonstrates the procedures utilized extensively in the next section.

3. Multi-scale equations for the hurricane embryo

Here we derive a system of multi-scale models which highlight the central dynamical features of the hurricane embryo in a simplified fashion. We begin with the balanced equations for fluctuations on the 10 km/15 min mesoscales.

3.1. *Balanced hot tower dynamics on microscales*

The derivation here involves straightforward scaling and is similar to the one in Majda *et al.* (2008). First, the order ϵ^{-1} contribution from the fluctuating part of the potential temperature equation in (2.2) yields the balance

$$N^2(z)w' = L\frac{\theta_0}{p_0}(C_d' - E_r'). \tag{3.1}$$

To derive the remaining equations for the microscale fluctuations, it is convenient to introduce the advection operator

$$\frac{\mathrm{D}'}{\mathrm{D}t'} = \frac{\partial}{\partial t} + (\bar{\boldsymbol{u}}_h + \boldsymbol{u}_h')\cdot\nabla_h' + w'\frac{\partial}{\partial z}, \tag{3.2}$$

which includes the mesoscale mean horizontal velocity. Note from (2.5) and (2.15) that the mesoscale vertical velocity is lower order. Inserting the ansatz from (2.5) into (2.2), the bounded leading-order terms satisfy the equations for microscale fluctuations:

$$\left.\begin{aligned}
\frac{\mathrm{D}'\boldsymbol{u}_h'}{\mathrm{D}t'} &= -\nabla_h' p' - w'\frac{\partial \bar{\boldsymbol{u}}_h}{\partial z} + \rho^{-1}(\rho\overline{\boldsymbol{u}_h' w'})_z,\\
\mathrm{div}_{\boldsymbol{x}}\boldsymbol{u}_h' + \rho^{-1}(\rho w')_z &= 0,\\
\frac{\mathrm{D}'q_v'}{\mathrm{D}t'} &= -C_d' + E_r' - w'\frac{\partial \bar{q}_v}{\partial z} + \rho^{-1}(\rho\overline{q_v' w'})_z,\\
\frac{\mathrm{D}'q_c'}{\mathrm{D}t'} &= C_d' - A_r' - w'\frac{\partial \bar{q}_c}{\partial z} + \rho^{-1}(\rho\overline{q_c' w'})_z,\\
\frac{\mathrm{D}'q_r'}{\mathrm{D}t'} - \frac{1}{\rho}\frac{\partial}{\partial z}(\rho V_t q_r') &= A_r' - E_r' - w'\frac{\partial \bar{q}_r}{\partial z} + \rho^{-1}(\rho\overline{q_r' w'})_z.
\end{aligned}\right\} \tag{3.3}$$

As emphasized in (2.5), the weaker potential temperature fluctuations $\epsilon\theta_1'$ can be determined afterwards from $\boldsymbol{q}'$, $\boldsymbol{u}_h'$, w' and p' by

$$\frac{\mathrm{D}'w'}{\mathrm{D}t'} = -p_z' + \theta_1' + (\bar{\epsilon}q_v' - q_c' - q_r') + \rho^{-1}(\rho\overline{w'^2})_z. \tag{3.4}$$

Note that when the large-scale advection effects are zero and the heat sources are prescribed, the equations in (3.1) and (3.3) reduce to the BHT models without rotation studied recently in Majda *et al.* (2008), where we have shown how a hot tower can generate large vorticity in a suitable preconditioning. We have obtained useful elementary insight into the role of hot towers in cyclogenesis, by carefully studying the role of various effects in generation, amplification, and dissipation of vorticity in hot towers. More detailed information can be found in Majda *et al.* (2008). Next, we develop simplified equations for the mesoscale variations of order 100 km on the fast, order 15 min time scale.

3.2. *Moist mesoscale wave dynamics*

The strength of the fluctuations in the potential temperature crucially affects the dynamics on the mesoscales and, in particular, the generation of moist gravity waves. First, in order to systematically implement the secularity conditions discussed at the

end of § 2, it is useful to rewrite the potential temperature equation from (2.2) in conservation form and then take the spatial average to obtain

$$\epsilon\frac{\partial\bar{\theta}_1}{\partial t}+\epsilon\frac{\partial\bar{\theta}}{\partial T}+\epsilon\mathrm{div}_{\boldsymbol{X}}(\bar{\boldsymbol{u}}_h\bar{\theta})+\epsilon^2\mathrm{div}_{\boldsymbol{X}}(\overline{\boldsymbol{u}_h'\theta_1'}) + \epsilon\rho^{-1}(\rho\bar{w}_1\bar{\theta})_z+\epsilon\rho^{-1}(\rho\overline{w'\theta_1'})_z+\frac{\partial\bar{\theta}}{\partial t}=\bar{S}_\theta-N^2\bar{w}_1. \tag{3.5}$$

There is a crucial assumption in (3.5), namely

Assumption 1:

$$\epsilon^{-1}\frac{L\theta_0}{p_0}(\bar{C}_d-\bar{E}_r)\equiv\bar{S}_\theta \text{ is bounded.} \tag{3.6}$$

Recall that with the non-dimensionalization in (2.2), the heating terms in (2.2) are allowed to have units of 30 K/15 min; on the microscales for BHT, such strong heating is consistent with the observed hot towers (Hendricks *et al.* 2004; Montgomery *et al.* 2006). Hot towers involve intense localized heating but their large-scale average mesoscale heating is much weaker and typically well within the 3 K/15 min bounds implied by (3.6). Assumption (3.6) allows for the weaker averaged mesoscale effects of sources from moisture of 3 K/15 min which is consistent in general with the weaker mesoscale impact of convection (Majda & Xing 2009, and references therein). With this assumption, from (3.5) we deduce that the leading-order bounded terms in (3.5) satisfy

$$\frac{\partial\bar{\theta}}{\partial t}=\bar{S}_\theta-N^2\bar{w}_1. \tag{3.7}$$

Equation (3.7) naturally yields the equation for fluctuations,

$$\frac{\partial\tilde{\bar{\theta}}}{\partial t}=\tilde{\bar{S}}_\theta-N^2\tilde{\bar{w}}_1. \tag{3.8}$$

On the other hand, the solvability condition for (3.7), $\langle\partial\bar{\theta}/\partial t\rangle=0$, to avoid secular terms in the expansion automatically imposes the requirement

$$N^2\langle\bar{w}_1\rangle=\langle\bar{S}_\theta\rangle, \tag{3.9}$$

which links the mesoscale time-averaged vertical velocity with the time-averaged heating from (3.6).

The non-zero temperature fluctuation in (3.8) drives hydrostatically balanced moist gravity waves. Since $\tilde{\bar{\theta}}\neq0$, the leading order ϵ^{-1} vertical momentum equation requires a hydrostatic pressure, $\epsilon^{-1}\bar{p}_{-1}$, in order to balance this effect, i.e.

$$(\bar{p}_{-1})_z=\tilde{\bar{\theta}}. \tag{3.10}$$

In similar fashion to that illustrated in (3.5) for the potential temperature, the order 1 momentum equation is given by Klein & Majda (2006) and Majda & Xing (2009):

$$\frac{\partial\bar{\boldsymbol{u}}_h}{\partial t}=-\nabla_{\boldsymbol{X}}\bar{p}_{-1}-\rho^{-1}(\rho\overline{w'\boldsymbol{u}_h'})_z. \tag{3.11}$$

Similarly, the order 1 moisture equations are

$$\left.\begin{aligned} \frac{\partial \bar{q}_v}{\partial t} &= -\bar{C}_d + \bar{E}_r - \rho^{-1}(\rho\overline{q_v' w'})_z, \\ \frac{\partial \bar{q}_c}{\partial t} &= \bar{C}_d - \bar{A}_r - \rho^{-1}(\rho\overline{q_c' w'})_z, \\ \frac{\partial \bar{q}_r}{\partial t} - \frac{1}{\rho}\frac{\partial}{\partial z}(\rho V_t \bar{q}_r) &= \bar{A}_r - \bar{E}_r - \rho^{-1}(\rho\overline{q_r' w'})_z. \end{aligned}\right\} \tag{3.12}$$

Equations (3.10), (3.11) and (3.12) together with

$$\left.\begin{aligned} \frac{\partial \tilde{\bar{\theta}}}{\partial t} &= \tilde{\bar{S}}_\theta - N^2 \tilde{\bar{w}}_1, \\ \mathrm{div}_{\boldsymbol{x}} \bar{\boldsymbol{u}}_h + \rho^{-1}(\rho \bar{w}_1)_z &= 0 \end{aligned}\right\} \tag{3.13}$$

constitute the MMW dynamics discussed earlier. These equations involve linear hydrostatic gravity wave dynamics and rapidly forced vertical vorticity modes on mesoscales driven by spatially averaged fluctuating heating and turbulent flux divergences from the microscales. The perceptive reader will notice that we still need equations for $\langle \bar{\boldsymbol{u}}_h \rangle$, $\langle \bar{\theta}_1 \rangle$, etc. in order to close the systems derived in §§ 3.1 and 3.2. We develop the long time mesoscale equations next to achieve this.

3.3. *Balanced mesoscale vortex dynamics*

First, we use the secularity constraint in (3.11), $\langle \partial \bar{\boldsymbol{u}}_h / \partial t \rangle = 0$, to derive the leading-order momentum equation

$$\nabla_{\boldsymbol{X}} \langle \bar{p}_{-1} \rangle = -\rho^{-1}(\rho \langle \overline{w' \boldsymbol{u}_h'} \rangle)_z, \tag{3.14}$$

while the time average of the hydrostatic balance constraint in (3.10) yields

$$\langle \bar{p}_{-1} \rangle_z = 0. \tag{3.15}$$

The only way to satisfy both (3.14) and (3.15) in general is to have a weaker time-averaged eddy momentum flux divergence and make

Assumption 2:

$$-\rho^{-1}(\rho \langle \overline{w' \boldsymbol{u}_h'} \rangle)_z = \epsilon \, \langle \bar{\boldsymbol{S}}_{\boldsymbol{u}} \rangle (\boldsymbol{X}, T), \tag{3.16}$$

which guarantees that (3.14) and (3.15) are automatically satisfied with $\langle \bar{p}_{-1} \rangle \equiv 0$. This justifies the ansatz for the pressure in (2.5) and guarantees that no secular gravity waves are generated on the mesoscales to leading order on the 2.5 h time scale. Similarly, averaging the moisture equations in (3.12) imposes the moisture source constraints:

$$\left.\begin{aligned} -\langle \bar{C}_d \rangle + \langle \bar{E}_r \rangle - \rho^{-1}(\rho \langle \overline{q_v' w'} \rangle)_z &= \epsilon \langle \bar{S}_{q_v} \rangle, \\ \langle \bar{C}_d \rangle - \langle \bar{A}_r \rangle - \rho^{-1}(\rho \langle \overline{q_c' w'} \rangle)_z &= \epsilon \langle \bar{S}_{q_c} \rangle, \\ \frac{1}{\rho}\frac{\partial}{\partial z}(\rho V_t \langle \bar{q}_r \rangle) + \langle \bar{A}_r \rangle - \langle \bar{E}_r \rangle - \rho^{-1}(\rho \langle \overline{q_r' w'} \rangle)_z &= \epsilon \langle \bar{S}_{q_r} \rangle \end{aligned}\right\} \tag{3.17}$$

for each vertical level z. These large-scale balances for the spatiotemporal averages in (3.16) and (3.17) need to be satisfied in order for the asymptotic procedure to remain valid; these equations are satisfied only if the space–time average is sufficiently weak, i.e. the appropriate large-scale space–time area fraction over the deep convective updrafts/downdrafts is sufficiently small (Klein & Majda 2006).

The derivation of the equations for the coarse-grained mesoscale averages is straightforward and only requires a repetition of the derivation for equations (3.6)–(3.10) from Majda (2007*a*). Thus time-averaging analysis for the order ϵ moisture equations yields

$$\left.\begin{aligned}\frac{\partial}{\partial T}\langle\bar{q}_v\rangle &= \langle\bar{S}_{q_v}\rangle - \mathrm{div}_X\langle\overline{q_v'\boldsymbol{u}_h'}\rangle - \frac{1}{\rho}\mathrm{div}(\rho\langle\bar{q}_v\bar{\boldsymbol{v}}\rangle),\\ \frac{\partial}{\partial T}\langle\bar{q}_c\rangle &= \langle\bar{S}_{q_c}\rangle - \mathrm{div}_X\langle\overline{q_c'\boldsymbol{u}_h'}\rangle - \frac{1}{\rho}\mathrm{div}(\rho\langle\bar{q}_c\bar{\boldsymbol{v}}\rangle),\\ \frac{\partial}{\partial T}\langle\bar{q}_r\rangle &= \langle\bar{S}_{q_r}\rangle - \mathrm{div}_X\langle\overline{q_r'\boldsymbol{u}_h'}\rangle - \frac{1}{\rho}\mathrm{div}(\rho\langle\bar{q}_r\bar{\boldsymbol{v}}\rangle),\end{aligned}\right\} \tag{3.18}$$

with $\bar{\boldsymbol{v}} = (\bar{\boldsymbol{u}}_h, \bar{w}_1)$. In similar fashion, the order ϵ mesoscale horizontal momentum equation becomes

$$\frac{\partial}{\partial T}\langle\bar{\boldsymbol{u}}_h\rangle + f\langle\bar{\boldsymbol{u}}_h\rangle^{\perp} = -\nabla_X\langle\bar{p}\rangle + \langle\bar{\boldsymbol{S}}_{\boldsymbol{u}}\rangle - \mathrm{div}_X\langle\overline{\boldsymbol{u}_h' : \boldsymbol{u}_h'}\rangle - \frac{1}{\rho}\mathrm{div}\langle\rho\bar{\boldsymbol{v}} : \bar{\boldsymbol{u}}_h\rangle \tag{3.19}$$

with $(\rho\boldsymbol{v} : \boldsymbol{u}_h)_i = \rho v u_{h,i}$ for $i = 1, 2$.

These equations for the mesoscale coarse-grained horizontal momentum are supplemented by (3.9) and the anelastic constraint,

$$\left.\begin{aligned} N^2\langle\bar{w}_1\rangle &= \langle\bar{S}_\theta\rangle,\\ \mathrm{div}_X\langle\bar{\boldsymbol{u}}_h\rangle + \rho^{-1}(\rho\langle\bar{w}_1\rangle)_z &= 0.\end{aligned}\right\} \tag{3.20}$$

Finally, the leading-order space–time average of the vertical momentum equation gives potential temperature fluctuations of the form $\epsilon\langle\bar{\theta}_1\rangle$ with

$$\langle\bar{\theta}_1\rangle = \langle p\rangle_z - \bar{\epsilon}\langle\bar{q}_v\rangle + \langle\bar{q}_c\rangle + \langle\bar{q}_r\rangle + \rho^{-1}\langle\rho\overline{w'^2}\rangle_z \tag{3.21}$$

in a similar fashion to that discussed earlier for the BHT dynamics (Majda *et al.* 2008). Equations (3.18), (3.19), (3.20) and (3.21) are the complete set for moist BMV dynamics.

The horizontal momentum equation (3.19) can be written in a more standard form by utilizing the identity

$$\frac{1}{\rho}\mathrm{div}\langle\rho\bar{\boldsymbol{v}} : \bar{\boldsymbol{u}}_h\rangle = \langle\bar{\boldsymbol{u}}_h\rangle\cdot\nabla_X\langle\bar{\boldsymbol{u}}_h\rangle + \langle\bar{w}_1\rangle\frac{\partial}{\partial z}\langle\bar{\boldsymbol{u}}_h\rangle + \frac{1}{\rho}\mathrm{div}\langle\rho\tilde{\bar{\boldsymbol{v}}} : \tilde{\bar{\boldsymbol{u}}}_h\rangle. \tag{3.22}$$

Thus, if we introduce the coarse-grained advective derivative

$$\frac{\mathrm{D}}{\mathrm{D}T} = \frac{\partial}{\partial T} + \langle\bar{\boldsymbol{u}}_h\rangle\cdot\nabla_X + \langle\bar{w}_1\rangle\frac{\partial}{\partial z}, \tag{3.23}$$

and use (3.22), the horizontal momentum equation from (3.19) becomes

$$\frac{\mathrm{D}}{\mathrm{D}T}\langle\bar{\boldsymbol{u}}_h\rangle + f\langle\bar{\boldsymbol{u}}_h\rangle^{\perp} = -\nabla_X\langle\bar{p}\rangle + \langle\bar{\boldsymbol{S}}_{\boldsymbol{u}}\rangle - \mathrm{div}_X\langle\overline{\boldsymbol{u}_h' : \boldsymbol{u}_h'}\rangle - \frac{1}{\rho}\mathrm{div}\langle\rho\tilde{\bar{\boldsymbol{v}}} : \tilde{\bar{\boldsymbol{u}}}_h\rangle. \tag{3.24}$$

The mesoscale averaged equations (3.20) and (3.24) are forced equations for rotating vertically sheared horizontal flow with mass sources as discussed in detail in Majda *et al.* (2008). These equations are driven by the space–time mesoscale averaged heat sources from (3.6) and (3.20), as well as eddy fluxes of momentum from both the microscale BHT dynamics and the MMW dynamics. The dynamical resemblance of BHT dynamics on the microscales from (2.1) and BMV dynamic equations on the mesoscales from (2.3) reflect the dynamical self-similarity principles discussed earlier (Majda 2007*b*; Majda *et al.* 2008; Majda & Xing 2009).

4. Simplified moist balanced hot tower models

The goal here is first to introduce a simplified set of equations describing the bulk microphysics in (2.3) yet capturing key features of deep convection qualitatively. Then axisymmetric moist hot tower solutions of the BHT equations from (3.1), (3.2) and (3.3) are developed to illustrate that these simpler models capture key features of moist deep convective dynamics qualitatively. In the same spirit of qualitative simplicity we utilize the approximation with constant entry throughout the remainder of the paper although this is not necessarily accurate for deep convection in a qualitative sense.

4.1. *Simplified cloud physics for deep convection*

Clouds form when the cloud vapour fraction, q_v, exceeds the saturation value, q_{vs}; in general, q_{vs} is determined by the Clausius–Clapeyron equation as a nonlinear function of temperature (Emanuel 1994; Klein & Majda 2006). For a typical averaged vertical profile of temperature, a mean sounding, $q_{vs}(z)$, is a decreasing function of height and this produces significant asymmetries between upward and downward motion in deep convection. Here, in the spirit of Boussinesq approximation, we assume that q_{vs} is a piecewise-linear decreasing function of height alone so that

$$q_{vs} = \begin{cases} q_{vs0} - \alpha_{vs} z, & \text{if } 0 \leqslant z \leqslant \dfrac{q_{vs0}}{\alpha_{vs}} \equiv 1.2, \\ 0, & \text{if } \dfrac{q_{vs0}}{\alpha_{vs}} < z. \end{cases} \tag{4.1}$$

Other key features to capture in a simplified cloud physics model are the latent heating of condensation, C_d, which causes air to rise and the evaporative cooling, E_r, of rain falling through subsaturated air which creates downdrafts. We make the simplest functional choices for the condensational heating, C_d, and evaporative cooling, E_r, consistent with this intuition,

$$\left.\begin{aligned} C_d &= \tau_d^{-1}(q_v - q_{vs}(z))^+, \\ E_r &= \tau_r^{-1}(q_{vs}(z) - q_v)^+ q_r. \end{aligned}\right\} \tag{4.2}$$

In (4.2) and below, $(*)^+$ denotes the non-negative part of the number $*$, while τ_d, τ_r are relaxation times for these two processes. The basic functional forms in (4.2) have similar qualitative features to much more complex bulk cloud microphysics models (Emanuel 1994; Grabowski & Smolarkiewicz 1996; Klein & Majda 2006). The mass fraction of cloud water, q_c, is typically an order of magnitude smaller than q_v and q_r with a rapid conversion process into rain; here we simplify the dynamics in (2.3) by imposing the steady state approximation, $C_d \equiv A_r$, which eliminates the cloud water, q_c, from the dynamics. The simplified equations for q_v and q_r in (2.3) with (4.1), (4.2) constitute the simplified cloud physics equations which are utilized in this section and the remainder of the paper. In these simplified models, the cloud water q_c, the water loading, is identified with $(q_v - q_{vs}(z))^+$, the saturation vapour excess.

Given an averaged mean vertical profile for moisture, $\bar{q}_v(z)$, there clearly should be a stronger potential for moist deeper convection to occur as the non-negative saturation deficit, $\delta = q_{vs}(z) - \bar{q}_v(z)$, decreases so the air is more moist. In the present context, for simplicity, we assume that

$$\bar{q}_v(z) = (q_{vs}(z) - \delta)^+, \tag{4.3}$$

where δ, the saturation deficit, is independent of height. Clouds are created in the mean environment when initially there is a bubble of moist air at low levels which

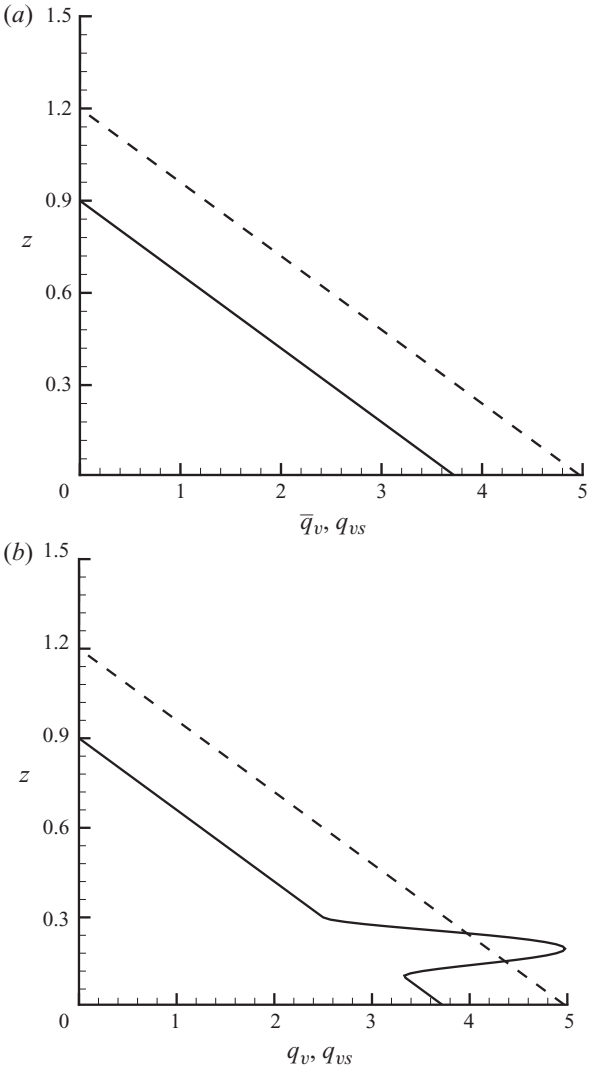

FIGURE 2. Illustration of $\bar{q}_v(z)$, $q_{vs}(z)$ and $q_v(z)$. (*a*) Plot of $\bar{q}_v(z)$ (solid) and $q_{vs}(z)$ (dashed) with $\delta = q_{vs0}/4$; (*b*) Plot of $q_v(z)$ (solid) and $q_{vs}(z)$ (dashed) with $a = \delta + 0.8$.

exceeds saturation (Grabowski & Smolarkiewicz 1996). Thus, the typical initial data that are used in the numerical studies here for deep hot tower development have the vertical structure

$$q_v^0 = \bar{q}_v(z) + q_v'(z), \qquad q_r^0 = 0, \tag{4.4}$$

where $q_v'(z)$ has support at low-levels above the boundary layer, between 1 and 3 km (i.e. 0.1 and 0.3). A simple choice for $q_v'(z)$ utilized below is

$$q_v'(z) = a\,(10(z-0.1))^2\,(10(z-0.3))^2\,, \tag{4.5}$$

which has maximum value a. See figure 2 for the graphical interpretation of (4.3), (4.4) and (4.5). How far the initial perturbation rises in the vertical and generates a shallow or deep hot tower depends on three factors:

Cloud physics parameters:

τ_d, τ_r, relaxation times; L, latent heat prefactor; V_T, falling velocity for rain. (4.6*a*)

Background vertical profile:

$$q_{vs}(z) \text{ and } \delta, \text{ saturation deficit in } \bar{q}_v(z). \tag{4.6b}$$

Initial perturbation parameter:

$$a, \text{ amplitude of perturbation}; \quad h_1, h_2, \text{ height of perturbation } q_v'(z). \tag{4.6c}$$

To focus on the effect of the background vertical profile and the cloud physics parameter, we always fix $a = 0.8 + \delta$, $h_1 = 0.1$, $h_2 = 0.3$, as illustrated in figure 2. This choice of a always guarantees a fixed amount of low-level cloud water independent of the saturation deficit, δ, in order to initiate a hot tower.

Here we assume that the moist BHT model derived in (3.1)–(3.3) operates on only the single scales of 10 km and 15 min, with the Boussinesq approximation, $\rho = 1$, and the simplified cloud physics in (4.2). Thus, these equations become the moist BHT model:

$$\left.\begin{aligned} \frac{\mathrm{D}\boldsymbol{u}_h}{\mathrm{D}t} &= -\nabla_h p, \\ \mathrm{div}_h \boldsymbol{u}_h + w_z &= 0, \\ w &= L(C_d - E_r), \\ \frac{\mathrm{D}q_v}{\mathrm{D}t} &= -C_d + E_r = -\frac{w}{L}, \\ \frac{\mathrm{D}q_r}{\mathrm{D}t} - \frac{\partial}{\partial z}(V_T q_r) &= C_d - E_r = \frac{w}{L}, \end{aligned}\right\} \tag{4.7}$$

with (4.2) for C_d, E_r and $\mathrm{D}/\mathrm{D}t = \partial/\partial t + \boldsymbol{u}_h \cdot \nabla_h + w\partial/\partial z$. Since the vertical velocity w in (4.7) is determined from (4.2) as a specific function of q_v and q_r, i.e.

$$w = L\left(\tau_d^{-1}(q_v - q_{vs}(z))^+ - \tau_r^{-1}(q_{vs}(z) - q_v)^+ q_r\right), \tag{4.8}$$

we can regard (4.7) as nonlinear hyperbolic equations for q_v, q_r with source terms nonlinearly coupled to the first three equations for vertically sheared horizontal flow in (4.7) (Majda *et al.* 2008). Note that from (4.8) there are updrafts (downdrafts) only for $q_v > q_{vs}(z)$, ($q_v < q_{vs}(z)$ and $q_r > 0$) with their magnitude controlled by τ_d^{-1} (τ_r^{-1}) individually and L overall. Also from the equations for q_v, q_r in (4.7), rising air depletes q_v (creates q_r) and descending air depletes q_r (creates q_v) in the simplified model. This provides simple intuition for the role of all the cloud physics parameters in (4.6) except the fall velocity of rain, V_T. Simple numerical experiments (omitted here) show that as V_T increases, the amount of rain q_r decays faster at any fixed vertical level while the magnitude of the downdrafts increases. Below, for illustration, we show results for the cloud physics parameters, $L = 0.24$, $V_T = 0.5$ (5 m s^{-1}), $\tau_r = \tau_d = 0.15$ which generate hot towers with reasonable vertical velocities in both updrafts and downdrafts.

4.2. *Axisymmetric moist hot towers in the BHT model*

Here we consider axisymmetric solutions of (4.7) so that q_v, q_r and w, $\boldsymbol{u}_h$ are functions of $r = |\boldsymbol{x}_h|$, z, t alone with $\boldsymbol{u}_h = u_r \boldsymbol{e}_r + u_\theta \boldsymbol{e}_\theta$ in usual cylindrical coordinates.

The conservation form for axisymmetric solutions of (4.7) becomes

$$\left.\begin{aligned} \frac{\partial(rq_v)}{\partial t}+\frac{\partial(ru_rq_v)}{\partial r}+\frac{\partial(rwq_v)}{\partial z} &= (-C_d+E_r)r,\\ \frac{\partial(rq_r)}{\partial t}+\frac{\partial(ru_rq_r)}{\partial r}+\frac{\partial(r(w-V_T)q_r)}{\partial z} &= (C_d-E_r)r,\\ w &= L(C_d-E_r),\\ u_r &= -\frac{1}{r}\int_0^r s\frac{\partial w}{\partial z}\,\mathrm{d}s,\\ \frac{\partial(ru_\theta)}{\partial t}+\frac{\partial(ru_ru_\theta)}{\partial r}+\frac{\partial(rwu_\theta)}{\partial z}+u_ru_\theta &= 0. \end{aligned}\right\} \tag{4.9}$$

Note that the first four of equations (4.9) determine axisymmetric hot towers in the BHT model and are solved completely independently from the last equation in (4.9) for angular momentum. Here we assume $u_\theta \equiv 0$ for simplicity. As in Majda *et al.* (2008), we can also study the effect of hot towers on ambient vorticity through the last equation in (4.9).

A first-order upwind finite volume scheme is employed to simulate (4.9) on a staggered grid. The domain size is set as $[0, 2] \times [0, 1.5]$. A grid of 200×200 computational cells is employed; a uniform vertical spacing is chosen and in the horizontal direction, a variable grid spacing with a very high resolution close to the centre is used which was defined according to $r_j = R\,(j/M)^2$ where $M = 200$ is the total number of grid points in the horizontal direction, r_j is the horizontal coordinate of the jth grid points and $R = 2$ is the radius of the modelled domain. A time step of $\Delta t = 0.00225$ was employed. No significant changes were observed with higher temporal or spatial resolutions. Extrapolation boundary conditions are used at all boundaries. To keep the two variables q_v, q_r non-negative, we impose $q_v = \max(q_v, 0)$, $q_r = \max(q_r, 0)$ after each time step (Grabowski & Smolarkiewicz 1996).

The initial data in all the numerical experiments have the form described earlier in (4.4) and (4.5) but with a cylindrical geometry so that

$$q_r^0 = 0, \qquad q_v^0 = \bar{q}_v(z) + q_v'(z)\phi(r), \tag{4.10}$$

with $q_v'(z)$ determined from (4.5) and $\phi(r) = \cos(\pi z)$ for $r < 0.5$ and zero otherwise. We utilize the fixed cloud physics parameters discussed below (4.8) with these initial data in a series of numerical experiments for axisymmetric plume dynamics described in the next paragraph. The value, q_{vs0}, from (4.1) is fixed at $q_{vs0} = 5$ and the saturation deficit is varied from $\delta = q_{vs0}/4$ to $\delta = q_{vs0}/32$ to $\delta = 0$ representing relatively dry, moist and saturated background profiles, respectively. The vertical velocity w and rain q_r for the developing axisymmetric hot towers in these three cases are shown in figures 3–6, at times $t = 1$, 2, 3, 5. In the case $\delta = q_{vs0}/4$ with the relatively dry troposphere from figure 3, the plume hardly rises with extremely weak velocities and negligible rainfall. For the case with $\delta = q_{vs0}/32$ with a moist troposphere from figures 4 and 5, the plume rises to nearly 6 km in this time interval with significant updraft velocities and some rainfall. The saturated case, $\delta = 0$ with a moist troposphere from figure 6, has significant vertical velocities and the hot tower rises to nearly 10 km in this time interval with significant rainfall, a factor of 4 larger than in figure 5. These three prototype simulations for axisymmetric moist hot towers in the BHT model mimic qualitatively what is expected for moist deep hot tower development in, respectively, a dry, moist and saturated mean background state in a qualitative fashion (Emanuel 1994) even though there is simplified cloud physics and balanced dynamics in the BHT model.

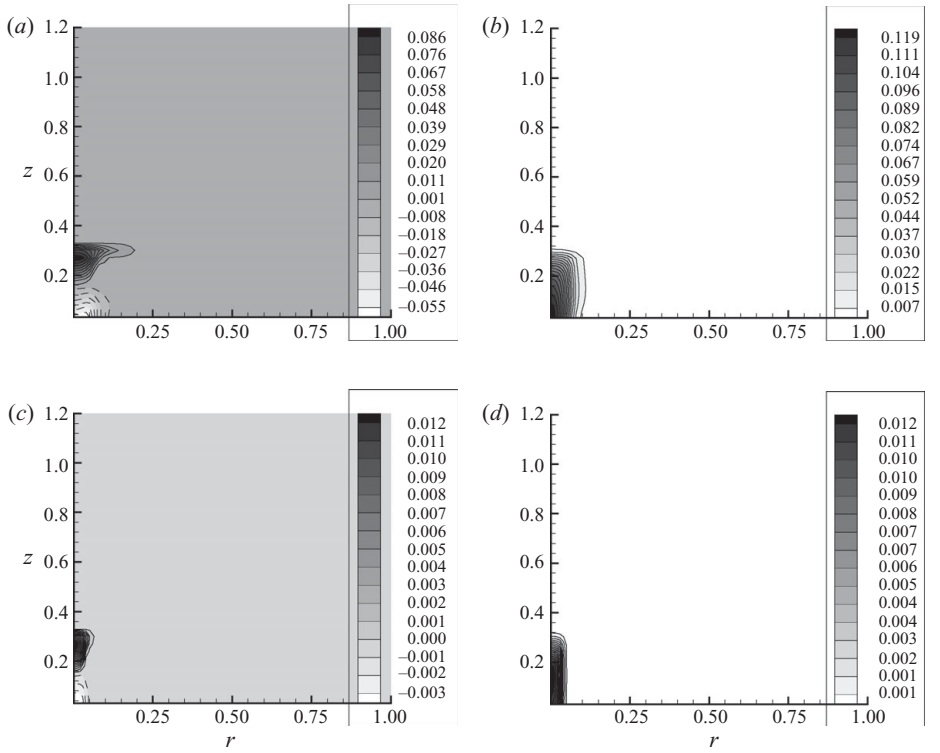

FIGURE 3. Contours and shading of the vertical velocity w and the mixing ratio of rain q_r at different times in the test case with $\delta = q_{vs0}/4$. (*a*, *b*) $t = 1$; (*c*, *d*) $t = 5$; (*a*, *c*) w; (*b*, *d*) q_r.

5. A prototype model: mesoscale vertical shear and microscale hot towers interacting in a vortical environment

The goal here is to utilize the simplified cloud models developed in § 4, together with the Boussinesq approximations $\rho \equiv 1$, $N^2 \equiv 1$ to illustrate solutions of the multi-scale model from § 3. The simplest setup which illustrates facets of the multi-scale system derived in § 3 is to utilize a periodic domain of length and width of order 100 km so that the mesoscale variables are just the non-zero mean values over the periodic box. Since in this special geometry, trivially $\mathrm{div}_{\boldsymbol{X}} \bar{\boldsymbol{u}}_h \equiv 0$, we need to enforce that the mesoscale vertical velocity $\bar{w}_1$ satisfies $\bar{w}_1 \equiv 0$; thus, we impose the requirements

$$\bar{S}_\theta = \epsilon^{-1} L(\bar{C}_d - \bar{E}_r) \qquad \text{and} \qquad \langle \bar{S}_\theta \rangle = O(\epsilon) \tag{5.1}$$

for self-consistency in periodic geometry. These are monitored diagnostically in the simulations below. Thus in the present context, the MMW equations from § 3.2 reduce to

$$\left.\begin{aligned} \frac{\partial \bar{\boldsymbol{u}}_h}{\partial t} &= -(\overline{w' \boldsymbol{u}'_h})_z, \\ \frac{\partial \bar{q}_v}{\partial t} &= -\bar{C}_d + \bar{E}_r - (\overline{q'_v w'})_z, \\ \frac{\partial \bar{q}_r}{\partial t} - \frac{\partial}{\partial z}(V_t \bar{q}_r) &= \bar{C}_d - \bar{E}_r - (\overline{q'_r w'})_z, \\ \frac{\partial \bar{\theta}}{\partial t} &= \bar{S}_\theta, \\ (\bar{p}_{-1})_z &= \tilde{\tilde{\theta}}. \end{aligned}\right\} \tag{5.2}$$

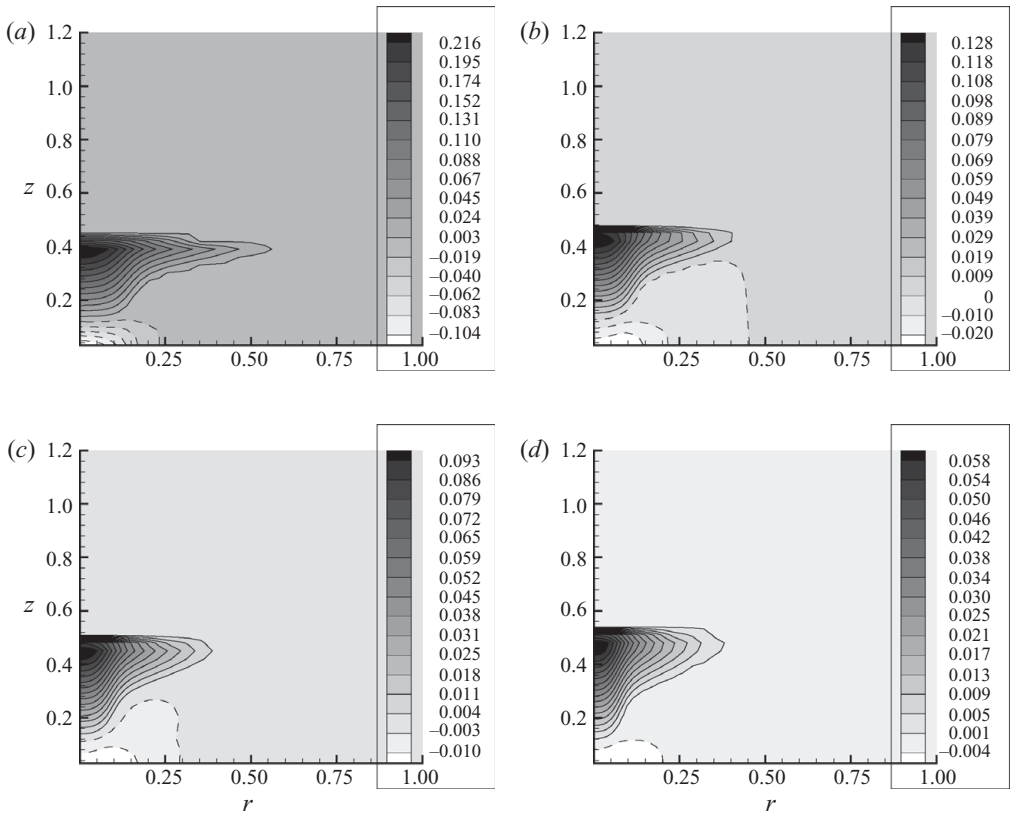

FIGURE 4. Contours and shading of the vertical velocity w at different times in the test case with $\delta = q_{vs0}/32$. (*a*) $t = 1$; (*b*) $t = 2$; (*c*) $t = 3$; (*d*) $t = 5$.

Note that the restoring forces due to buoyancy are absent, and no gravity waves are generated in this special environment. Similarly, the large-scale BMV dynamics derived in § 3.3 satisfies $\bar{w}_1 \equiv 0$ so that the BMV dynamics in periodic geometry assumes the simple form:

$$\left.\begin{aligned} \frac{\partial \boldsymbol{U}_h}{\partial T} + f\boldsymbol{U}_h^{\perp} &= -(\langle \overline{w'\boldsymbol{u}_h'} \rangle)_z, \qquad \boldsymbol{U}_h(z,t) = \langle \bar{\boldsymbol{u}}_h \rangle, \\ \frac{\partial}{\partial T}\langle \bar{q}_v \rangle &= -\langle \bar{C}_d \rangle + \langle \bar{E}_r \rangle - (\langle \overline{q_v' w'} \rangle)_z, \\ \frac{\partial}{\partial T}\langle \bar{q}_r \rangle - \frac{\partial}{\partial z}\left(V_t \langle \bar{q}_r \rangle\right) &= \langle \bar{C}_d \rangle - \langle \bar{E}_r \rangle - (\langle \overline{q_r' w'} \rangle)_z, \\ \langle \bar{\theta}_1 \rangle &= \langle p \rangle_z - \bar{\epsilon}\langle \bar{q}_v \rangle + \langle \bar{q}_r \rangle + \rho^{-1}\langle \rho \overline{w'^2} \rangle_z. \end{aligned}\right\} \tag{5.3}$$

Thus, the BMV dynamics in this special set-up allows for large-scale vertical shears which respond to both eddy momentum flux divergences and the effects of rotation. In the present context, the BHT dynamics for microscale fluctuations from § 3.2

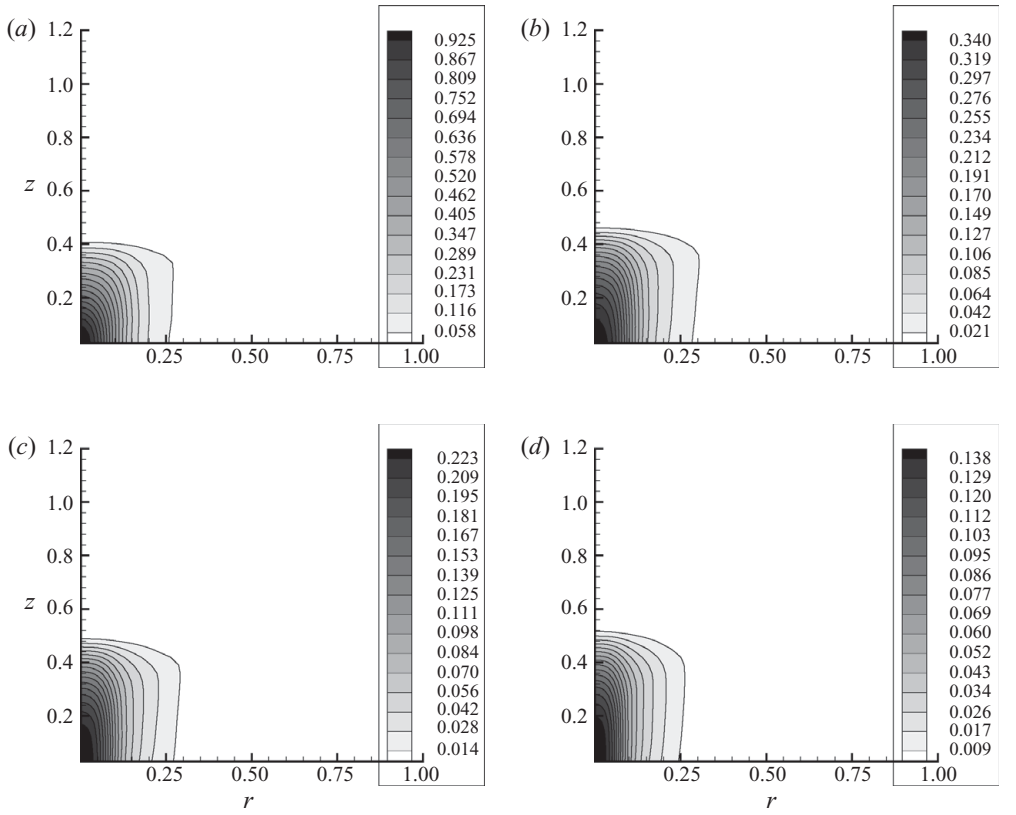

FIGURE 5. Contours and shading of the mixing ratio of rain q_r at different times in the test case with $\delta = q_{vs0}/32$. (*a*) $t = 1$; (*b*) $t = 2$; (*c*) $t = 3$; (*d*) $t = 5$.

becomes

$$\left.\begin{aligned}
\frac{\mathrm{D}\boldsymbol{u}_h'}{\mathrm{D}t'} &= -\nabla_h p' - w'\frac{\partial \bar{\boldsymbol{u}}_h}{\partial z} + (\overline{\boldsymbol{u}_h' w'})_z,\\
\mathrm{div}_{\boldsymbol{x}}\boldsymbol{u}_h' + w_z' &= 0,\\
w' &= L(C_d' - E_r'),\\
\frac{\mathrm{D}'q_v'}{\mathrm{D}t'} &= -C_d' + E_r' - w'\frac{\partial \bar{q}_v}{\partial z} + (\overline{q_v' w'})_z,\\
\frac{\mathrm{D}'q_r'}{\mathrm{D}t'} - \frac{\partial}{\partial z}(V_t q_r') &= C_d' - E_r' - w'\frac{\partial \bar{q}_r}{\partial z} + (\overline{q_r' w'})_z,\\
\frac{\mathrm{D}}{\mathrm{D}t'} &= \frac{\partial}{\partial t} + (\bar{\boldsymbol{u}}_h + \boldsymbol{u}_h')\cdot\nabla_h + w'\frac{\partial}{\partial z}.
\end{aligned}\right\} \tag{5.4}$$

Equations (5.2)–(5.4) are the simplified model dynamics studied here. The effect of mesoscale vertical shears on cyclogenesis in the hurricane embryo is an important practical topic (Emanuel 1989; Hendricks *et al.* 2004; Montgomery *et al.* 2006) and the advection by the shear in (5.4) for the microscale BHT dynamics as well as the feed back on the mesoscale shear in (5.2) and (5.3) give a simplified balanced context for this effect in the embryo. Here we simply use this model to demonstrate coupled multi-scale behaviour in this prototype setting. Of course, we need to check the required

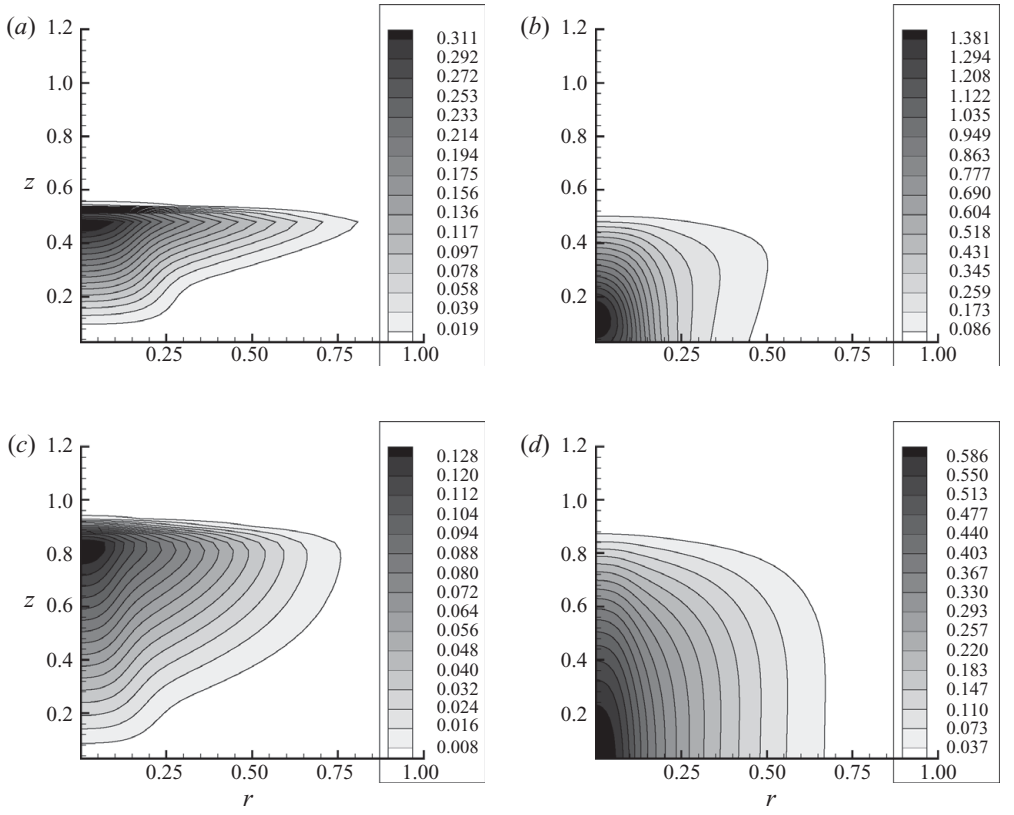

FIGURE 6. Contours and shading of the vertical velocity w and the mixing ratio of rain q_r at different times in the test case with $\delta = 0$. (a, b) $t = 1$; (c, d) $t = 5$; (a, c) w; (b, d) q_r.

self-consistency from *Assumption 2* in (3.16) and (5.2) as time proceeds in order to ensure the asymptotic validity of the model equations. The simulations below begin with a background moisture profile with a given saturation deficit, $\delta \geqslant 0$; $\delta = q_{vs0}/32$ is used below. Perturbations of the low-level moisture with the same form $q_v'(z)\phi(r)$ from (4.4)–(4.6) and (4.10) at random locations, $\boldsymbol{x}_j$, with $r = |\boldsymbol{x} - \boldsymbol{x}_j|$ are added every 10 units (2.5 h) to mimic the seeding of random hot towers as illustrated earlier in § 4.2.

5.1. *Vertical vorticity budgets and the numerical methods*

Obviously, the main dynamical core in the numerics involves the solution of (5.4). To solve this equation numerically, we utilize (Majda *et al.* 2008) the horizontal Helmholtz decomposition

$$\left.\begin{aligned} \boldsymbol{u}_h' &= \nabla_h \Phi + \nabla_h^{\perp} \Psi, \\ \Delta \Psi &= \omega', \qquad \omega' \text{ vertical vorticity}, \\ \Delta \Phi &= \mathrm{div}_{\boldsymbol{x}} \boldsymbol{u}_h' = -w_z', \end{aligned}\right\} \tag{5.5}$$

and take the horizontal curl of (5.4) to obtain the vertical vorticity equation

$$\frac{\partial \omega'}{\partial t} + (\bar{\boldsymbol{u}}_h + \boldsymbol{u}_h') \cdot \nabla_h \omega' + w' \omega_z' = \omega' w_z' - \nabla_h^{\perp} w' \cdot (\bar{\boldsymbol{u}}_h + \boldsymbol{u}_h')_z \tag{5.6}$$

with w' specified through the third equation in (5.4). The two quadratic terms on the left-hand side of (5.6) represent horizontal and vertical advection of vorticity, respectively. The terms on the right-hand side represent the production terms for vertical vorticity with $\omega' w'_z$ the important vortex stretching term and the remaining term, $-\nabla_h^{\perp} w' \cdot (\bar{\boldsymbol{u}}_h + \boldsymbol{u}'_h)_z$ defining the vertical tilt (Montgomery *et al.* 2006). Majda *et al.* (2008) study a variety of elementary exact solutions illustrating these competing effects in the balanced model with specified heating from hot towers. There is direct feedback and interactions with the large scale through the equation in (5.3) for the mean moisture and temperature. The couple equations in (5.3) and (5.4) are what are actually solved in all the numerics below.

The numerical method for solving (5.5), (5.6) consists of two fast spectral Poisson solvers for (5.5) at each horizontal level of a regularly spaced vertical grid coupled with standard horizontal pseudospectral methods for the horizontal advection in (5.6) while the vertical advection and integration for (5.6) is done by utilizing a second-order accurate upwind scheme on the vertical grid (Mohammadian & LeRoux 2008) together with the boundary conditions $w'|_{z=0,H} = 0$ at the top and bottom of the troposphere. Here the height of the troposphere, H, is given by 1.5, i.e. 15 km. For numerical purposes, in standard fashion, horizontal hyperviscosity $-\mu_4 \nabla^4 \omega'$ is added to the right-hand side of (5.6) with $\mu_4 = D_4 (K_{max}^4 \Delta t)^{-1}$, Δt the time step and $K_{max}^2 = (\pi/\Delta x)^2 + (\pi/\Delta y)^2$. Careful numerical experiments with the elementary plumes yield the value $D_4 = 0.1$, which ensures stability with minimal dissipation for the mesh sizes used below. Time discretization is by a fourth-order Runge–Kutta method. The cloud physics equations in (5.3) and (5.4) are solved by the same upwind scheme utilized in § 4.

The simple multi-scale ordinary differential equations in (5.2) and (5.3) are solved by a standard multi-time scale integrator since (5.2) occurs on the fast time scale while (5.3) involves evolution on the long time scale (Grabowski 2004; Majda & Stechmann 2009; Xing *et al.* 2009). A few brief comments are made here. A coarse time step for (5.3), ΔT, is utilized with $\Delta T = n \Delta t$ with Δt the fine scale time step for (5.2) and (5.4). For illustration, consider the horizontal momentum. The fluctuations $\tilde{\tilde{\boldsymbol{u}}}_h$ are solved through (5.2) and updated each fine time step Δt while the coarse-grained averages, $\boldsymbol{U}_h$, in (5.3) are updated every coarse time step ΔT through the empirical time average of the turbulent flux divergence on the right-hand side of (5.3) over the n-small-scale time steps. The representative value $\epsilon = 0.1$ is utilized in the present algorithm so that $n = 10$ and $\bar{\boldsymbol{u}}_h$ is calculated at each small-scale time step by the decomposition, $\bar{\boldsymbol{u}}_h = \boldsymbol{U}_h + \tilde{\tilde{\boldsymbol{u}}}_h$, from (2.9). The fourth-order Runge–Kutta method is used for both coarse and fine scale time steps. This completes the numerical method.

5.2. *Prototype simulations*

Some simple prototype numerical simulations are shown in this subsection to briefly illustrate features in the models. We choose the length and width of the periodic domain as 12.8, i.e. 128 km, and the height of the troposphere as 1.5, i.e. 15 km. The resolutions in the horizontal and vertical direction are 0.1 and 0.075, respectively, i.e. 1 km horizontal and 0.75 km vertical resolution. The large-scale time step ΔT is set as 0.1, and the small-scale time step $\Delta t = \epsilon \Delta T$ is 0.01. The Coriolis effect coefficient is given by the value at 25°N, $\sin(25\pi/180)$. The numerical simulations are performed for 400 units, i.e. 100 h. The initial conditions of the numerical test are given by

$$\omega'_0 = 0, \qquad V_0 = 0, \qquad \tilde{\tilde{u}}_0 = \tilde{\tilde{v}}_0 = 0, \qquad u' = v' = 0, \tag{5.7}$$

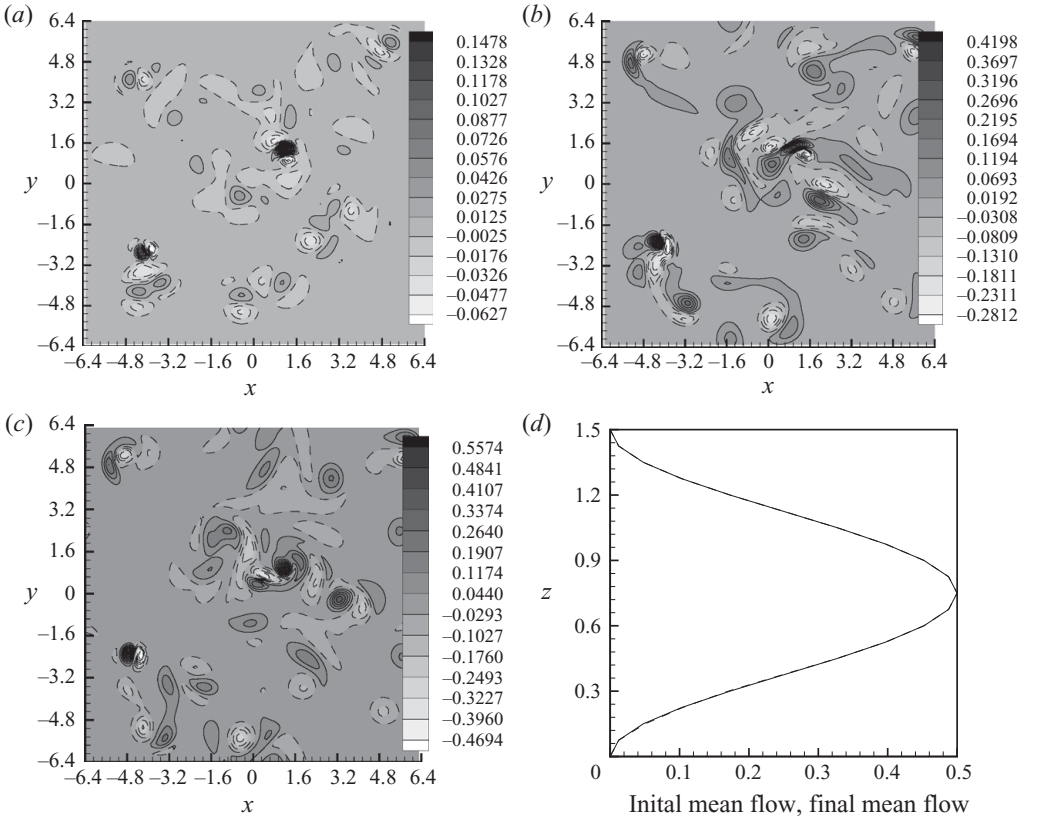

FIGURE 7. Contours and shading of small-scale vertical vorticity at time 400 for the test with $\omega_0 = 0$, $U_0 = 0.25 - s0.25\cos(2\pi z/1.5)$ and saturation deficit $\delta = q_{vs0}/32$. Solid contour lines represent positive values and dashed ones represents negative values. The results correspond to the following levels: $z = 0.15$ (a), $z = 0.3$ (b), $z = 0.45$ (c). The vorticity at the level 0.6 is zero. (d) Comparison of the initial (solid) and final (dashed) mean velocity $\sqrt{\bar{u}^2 + \bar{v}^2}$. Note the overlap of the initial and final velocity.

with the initial value $U_0 = 0.25 - 0.25\cos(2\pi z/1.5)$ and the moist background profile with saturation deficit $q_{vs0}/32$. From (5.6), the net circulation always vanishes over the entire period box, so more subtle statistics are needed to see the buildup of low-level cyclonic vorticity. We compute the skewness of vorticity for the whole ensemble of data during the immediate past 48 time units. This skewness is defined by

$$\gamma = \frac{\mu_3}{\sigma^3} = \frac{\sqrt{n}\sum_{i=1}^{n}(\omega_i' - \overline{\omega'})^3}{\left(\sum_{i=1}^{n}(\omega_i' - \overline{\omega'})^2\right)^{3/2}}, \tag{5.8}$$

and $n = 48$ is utilized here; a positive skewness with an increasing amplitude reflects preferred cyclonic activity.

A snapshot of the vorticity field in this numerical solution at time $T = 400$ is given in figure 7 at the levels 0.15, 0.3 and 0.45 corresponding to 1.5, 3 and 4.5 km. The vorticity is 0–4 significant figures above the level of 6 km since the hot towers with

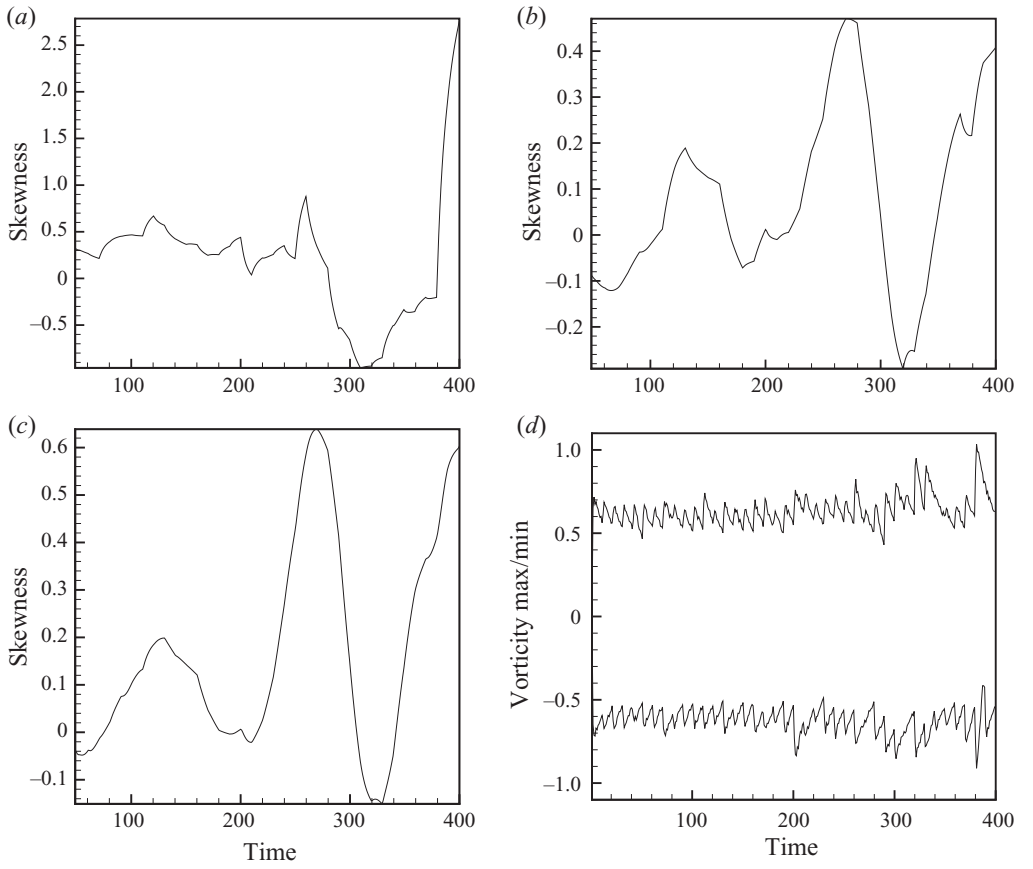

FIGURE 8. Skewness of small-scale vertical vorticity at different times for the test with $\omega_0 = 0$, $U_0 = 0.25 - 0.25\cos(2\pi z/1.5)$ and saturation deficit $\delta = q_{vs0}/32$. The results correspond to the following levels: $z = 0.15$ (*a*), $z = 0.3$ (*b*), $z = 0.45$ (*c*). Note the cyclonic skewness at low levels. (*d*) Time history of vorticity maximum/minimum at $z = 0.45$.

this saturation deficit, $\delta = q_{vs0}/32$, rarely rise above this level as shown earlier in figure 4. There is a clear buildup of more intense cyclonic vorticity as depicted in figure 7. This is confirmed by the skewness plots in figure 8 which show a buildup of significant positive skewness for most of the time interval. Figure 8(*d*) shows the intensifying vorticity extrema. Figure 7(*d*) shows that the turbulent eddy momentum flux divergences have a negligible effect on the mean momentum with similar results (not shown) for the mean background moisture profile which is essentially unchanged. We perform the same test with a different shear flow $U_0 = 0.25 + 0.25\sin(2\pi z/1.5)$ and observe that the skewness is mostly negative or slightly positive for the 400 units of the simulation time. Hence this rotating shear has created a favourable background for cyclonic vorticity. This simulation is an example with features of the vertical hot tower scenario of Montgomery *et al.* (2006). Other numerical simulations (Zhang & Bao 1996) and theory (Majda *et al.* 2008) support enhanced cyclonic vorticity generation at low levels as we see here in the prototype simulation.

6. Concluding discussions

Three simplified interacting moist multi-scale models for the hurricane embryo have been developed in § 3 through systematic principles. These models isolate key dynamical aspects of the hurricane embryo: the BMV model includes explicit effects of rotation, nonlinear advection, upscale heating from moist convection and turbulent momentum fluxes in a simple balanced model for mesoscale vortex intensification; the microscale BHT model is a simplified balanced model for moist hot towers and vortex dynamics in an interacting moist mesoscale environment; the MMW model includes the impact of short time scale but spatial mesoscale fluctuations of moisture and hydrostatically balanced gravity waves. The role of such simplified dynamical models in understanding detailed moist hot tower dynamics has been illustrated in § 4 and § 5. A simplified cloud physics model for deep convection was introduced in § 4 and used to study moist axisymmetric plumes in an ambient background with varying moisture. The simulations in § 5 illustrate the development of intense low-level cyclonic fluctuations through moist BHTs with simplified cloud physics through multi-scale balanced dynamics. Thus, the simplified models developed here capture several of the features, in a qualitative fashion, observed in numerical simulations of comprehensive models for the hurricane embryo (Hendricks *et al.* 2004; Montgomery *et al.* 2006). Future research directions involve further development of the analytic properties of the models with active moisture effects, and their potential use as diagnostic and predictive models for key mechanisms for cyclogenesis in the hurricane embryo.

The research of A.J.M. is partially supported by the National Science Foundation grant DMS-0456713 and the Office of Naval Research grant N00014-05-1-0164. Y.X. has been supported as a post-doctoral fellow through these grants.

REFERENCES

Biello, J. A. & Majda, A. J. 2005 A new multiscale model for the Madden–Julian oscillation. *J. Atmos. Sci.* **62**, 1694–1721.

Biello, J. A. & Majda, A. J. 2006 Modulating synoptic scale convective activity and boundary layer dissipation in the IPESD models of the Madden–Julian oscillation. *Dyn. Atmos. Oceans* **42**, 152–215.

Biello, J. A. & Majda, A. J. 2009 Intraseasonal multi-scale moist dynamics of the tropical troposphere. *Commun. Math. Sci.* **8**, 519–540.

Biello, J. A., Majda, A. J. & Moncrieff, M. W. 2007 Meridional momentum flux and superrotation in the multi-scale IPESD MJO model. *J. Atmos. Sci.* **64**, 1636–1651.

Dunkerton, T. J., Montgomery, M. T. & Wang, Z. 2008 Tropical cyclogenesis in a tropical wave critical layer: easterly waves. *Atmos. Chem. Phys. Discuss.* **8**, 11149–11292.

Emanuel, K. A. 1989 The finite-amplitude nature of tropical cyclogenesis. *J. Atmos. Sci.* **46**, 3431–3456.

Emanuel, K. A. 1994 *Atmospheric Convection*. Oxford University Press.

Frank, W. M. & Roundy, P. E. 2006 The role of tropical waves in tropical cyclogenesis. *Mon. Wea. Rev.* **134**, 2397–2417.

Grabowski, W. W. 2001 Coupling cloud processes with the large-scale dynamics using the cloud-resolving convection parameterization (CRCP). *J. Atmos. Sci.* **58**, 978–997.

Grabowski, W. W. 2004 An improved framework for superparameterization. *J. Atmos. Sci.* **61**, 1940–1952.

Grabowski, W. W. & Smolarkiewicz, P. K. 1996 Two-time-level semi-Lagrangian modeling of precipitating clouds. *Mon. Weather Rev.* **124**, 487–497.

Hendricks, E. A., Montgomery, M. T. & Davis, C. A. 2004 The role of "vortical" hot towers in the formation of tropical cyclone Diana (1984). *J. Atmos. Sci.* **61**, 1209–1232.

Klein, R. 2000 Asymptotic analyses for atmospheric flows and the construction of asymptotically adaptive numerical methods. *Z. Angew. Math. Mech.* **80**, 765–777.

Klein, R. & Majda, A. J. 2006 Systematic multiscale models for deep convection on mesoscales. *Theor. Comput. Fluid Dyn.* **20**, 525–551.

Lipps, F. B. & Hemler, R. S. 1982 A scale analysis of deep moist convection and some related numerical calculations. *J. Atmos. Sci.* **39**, 2192–2210.

Majda, A. J. 2003 *Introduction to PDEs and Waves for the Atmosphere and Ocean.* Courant Lecture Notes in Mathematics, vol. 9. American Mathematical Society.

Majda, A. J. 2007*a* Multiscale models with moisture and systematic strategies for superparameterization. *J. Atmos. Sci.* **64**, 2726–2734.

Majda, A. J. 2007*b* New multiscale models and self-similarity in tropical convection. *J. Atmos. Sci.* **64**, 1393–1404.

Majda, A. J. & Biello, J. A. 2004 A multiscale model for tropical intraseasonal oscillation. *Proc. Natl Acad. Sci. USA* **101**, 4736–4741.

Majda, A. J. & Klein, R. 2003 Systematic multiscale models for the tropics. *J. Atmos. Sci.* **60**, 393–408.

Majda, A. J., Mohammadian, M. & Xing, Y. 2008 Vertically sheared horizontal flow with mass sources: a canonical balanced model. *Geophys. Astrophys. Fluid Dyn.* **102**, 543–591.

Majda, A. J. & Stechmann, S. 2009 A simple dynamic model with features of convective momentum transport. *J. Atmos. Sci.* **66**, 373–392.

Majda, A. J. & Xing, Y. 2009 New multi-scale models on mesoscales and squall lines. *Commun. Math. Sci.* **8**, 113–134.

Mohammadian, A. M. & LeRoux, D. Y. 2008 Fourier analysis of a class of upwind schemes in shallow water systems for gravity and Rossby waves. *Intl J. Numer. Methods Fluids* **57**, 389–416.

Molinari, J., Lombardo, K. & Vollaro, D. 2007 Tropical cyclogenesis within an equatorial Rossby wave packet. *J. Atmos. Sci.* **64**, 1301–1317.

Molinari, J., Vollaro, D. & Corbosiero, K. L. 2004 Tropical cyclone formation in a sheared environment: a case study. *J. Atmos. Sci.* **61**, 2493–2509.

Montgomery, M. T., Nicholls, M. E., Cram, T. A. & Saunders, A. B. 2006 A vortical hot tower route to tropical cyclogenesis. *J. Atmos. Sci.* **63**, 355–386.

Nolan, D. S. 2007 What is the trigger for tropical cyclogenesis? *Aust. Meteorol. Mag.* **56**, 241–266.

Ritchie, E. A. & Holland, G. J. 1997 Scale interactions during the formation of Typhoon Irving. *Mon. Weather Rev.* **125**, 1377–1396.

Sobel, A. H., Nilsson, J. & Polvani, L. M. 2001 The weak temperature gradient approximation and balanced tropical moisture waves. *J. Atmos. Sci.* **58**, 3650–3665.

Xing, Y., Majda, A. J. & Grabowski, W. W. 2009 New efficient sparse space-time algorithms for superparameterization on mesoscales. *Mon. Weather Rev.* **137**, 4307–4324.

Zhang, D.-L. & Bao, N. 1996 Oceanic cyclogenesis as induced by a mesoscale convective system moving offshore. Part II. Genesis and thermodynamic transformation. *Mon. Weather Rev.* **124**, 2206–2225.